



## RESEARCH ARTICLE

10.1029/2021JG006520

# Unraveling the Contribution of Turbulence and Bubbles to Air-Water Gas Exchange in Running Waters

M. Klaus<sup>1</sup> , T. Labasque<sup>2</sup>, G. Botter<sup>3</sup> , N. Durighetto<sup>3</sup> , and J. Schelker<sup>4,5</sup> 

<sup>1</sup>Department of Forest Ecology and Management, Swedish University of Agricultural Sciences, Umeå, Sweden, <sup>2</sup>Géosciences Rennes, Université Rennes, CNRS, Rennes, France, <sup>3</sup>Department of Civil Architectural and Environmental Engineering, University of Padova, Padova, Italy, <sup>4</sup>WasserCluster Lunz - Biological Station, Lunz am See, Austria, <sup>5</sup>Department of Functional and Evolutionary Ecology, University of Vienna, Vienna, Austria

### Key Points:

- Air–water gas exchange rates in bubbly running waters follow the same mechanistic scaling laws as in oceans
- Bubble life and equilibration times are critical for accurate scaling of gas exchange rates
- Key drivers of gas exchange correlate with ambient sound spectral signatures

### Supporting Information:

Supporting Information may be found in the online version of this article.

### Correspondence to:

M. Klaus,  
marcus.klaus@posteo.net

### Citation:

Klaus, M., Labasque, T., Botter, G., Durighetto, N., & Schelker, J. (2022). Unraveling the contribution of turbulence and bubbles to air–water gas exchange in running waters. *Journal of Geophysical Research: Biogeosciences*, 127, e2021JG006520. <https://doi.org/10.1029/2021JG006520>

Received 6 JUL 2021  
Accepted 26 JAN 2022

### Author Contributions:

**Conceptualization:** M. Klaus, T. Labasque, G. Botter, N. Durighetto, J. Schelker  
**Data curation:** M. Klaus  
**Formal analysis:** M. Klaus  
**Funding acquisition:** M. Klaus, T. Labasque, J. Schelker  
**Investigation:** M. Klaus, T. Labasque, N. Durighetto, J. Schelker  
**Methodology:** M. Klaus, T. Labasque, J. Schelker  
**Project Administration:** M. Klaus, J. Schelker

© 2022. The Authors.

This is an open access article under the terms of the [Creative Commons Attribution-NonCommercial-NoDerivs License](https://creativecommons.org/licenses/by/4.0/), which permits use and distribution in any medium, provided the original work is properly cited, the use is non-commercial and no modifications or adaptations are made.

**Abstract** Quantifying air–water gas exchange is critical for estimating greenhouse gas fluxes and metabolism in aquatic ecosystems. In high-energy streams, the gas exchange rate  $k$  is poorly constrained, due to an incomplete understanding of turbulence and bubble contributions to  $k$ . We performed a flume experiment with air bubble additions to evaluate the combined effects of turbulence and bubbles on  $k$  for helium, argon, xenon, and methane. We created contrasting hydraulic conditions by varying channel slope, bed roughness, water discharge, and bubble flux. We found that  $k$  increased from 1–4 to 17–66 m d<sup>-1</sup> with increases in turbulence and bubble flux metrics. Mechanistic models that explicitly account for these metrics, as well as gas diffusivity and solubility, agreed well with the data and indicated that bubble-mediated gas exchange accounted for 64–93% of  $k$ . Bubble contributions increased with bubble flux but were independent of gas type, as bubbles did not equilibrate with the water. This was evident through modeled bubble life and equilibration times inferred from bubble size distributions obtained from underwater sound spectra. Sound spectral properties correlated well with turbulence and bubble flux metrics. Our results demonstrate that (a) mechanistic models can be applied to separate free surface- and bubble-mediated gas exchange in running waters, (b) bubble life and equilibration times are critical for accurate scaling of  $k$  between different gases, and (c) ambient sound spectra can be used to approximate contributions of turbulence and bubbles.

**Plain Language Summary** Aquatic systems exchange gases with the atmosphere and this exchange is important for many fundamental ecosystem processes and the global greenhouse gas cycle. How fast gases exchange with the atmosphere is, however, difficult to determine, especially in streams and rivers where bubbles can speed up the exchange of certain gases. Here, we used experimental stream channels to create a wide range of flow conditions, and test how these conditions affect the rate at which different gases in the water exchange with the atmosphere. We found that irregular water motions and bubbles generally enhance gas exchange and that these effects can be described by physical equations of flow and bubble characteristics in similar ways as previously shown in oceans. The equations can be used to quantify the specific contribution of bubbles to gas exchange and this can be important when comparing exchange rates of different gases such as carbon dioxide and oxygen. We also find that important drivers of gas exchange can be derived from flow and bubble sound recorded by microphones. In essence, we provide new equations and field methods that will improve our understanding and ability to quantify gas exchange processes in streams and rivers.

## 1. Introduction

Air–water gas exchange is crucial for aquatic ecosystems as it affects metabolic fluxes, elemental cycling, and the exchange of greenhouse gases (GHGs) with the atmosphere (Laursen & Seitzinger, 2005; Likens, 2010; McCutchan et al., 1998; Raymond et al., 2013). The flux across the air–water interface is described by Fick's first law of diffusion where  $Flux = k(C_w - C_{eq})$ , is the surface water gas concentration,  $C_w$  is the air–equilibrium gas concentration and  $k$  is the air–water gas exchange rate. The  $k$  can be regarded as the water column depth that equilibrates with the atmosphere per unit time. Recent studies have highlighted exceptionally high  $k$  in steep mountain streams (Hall & Madinger, 2018; Ulseth et al., 2019). Such streams are widespread across the earth (Larsen et al., 2014) and high  $k$  contributes to globally relevant GHG emissions (Horgby et al., 2019; Qu et al., 2017). However, these gas exchange estimates remain uncertain because  $k$  is inadequately constrained in mountain streams due to a poor understanding of the underlying physical drivers.

**Resources:** M. Klaus, T. Labasque, J. Schelker  
**Software:** M. Klaus  
**Supervision:** G. Botter, J. Schelker  
**Validation:** M. Klaus, G. Botter  
**Visualization:** M. Klaus  
**Writing – original draft:** M. Klaus  
**Writing – review & editing:** M. Klaus, T. Labasque, G. Botter, N. Durighetto, J. Schelker

Traditionally, variations of  $k$  for sparingly soluble gases have been assumed to result from irregular water motions near the water surface. In streams, this near-surface turbulence is caused by interactions between water flow and streambed structures and increases with channel roughness, slope, and flow velocity/discharge (Moog & Jirka, 1999; Raymond et al., 2012). These effects lead to the dissipation of turbulent kinetic energy, which in turn scales with  $k$  (Moog & Jirka, 1999; Wang et al., 2021; Zappa et al., 2007). Recently, Ulseth et al. (2019) suggested that the scaling of  $k$  with turbulent kinetic energy dissipation follows two distinct regimes. In low-energy streams, turbulence acts as the dominant driver of gas exchange across the free water surface, while in high-energy systems, gas exchanges predominantly through bubbles. Bubbles become typically entrained at the water surface in cascades or waterfalls and are then carried downstream until they resurface. They provide extended exchange surfaces between air and water and thus can enhance  $k$  by several orders of magnitude (Chanson, 1995; Cirpka et al., 1993). The contribution of gas exchange in running waters across the free water surface and through bubble surfaces has been described by mechanistic  $k$  models, but these models are limited to specific flow conditions occurring at characteristic hydraulic features (Chanson, 1995; Cirpka et al., 1993; Lakso, 1988). Generic mechanistic models that explicitly account for free surface- and bubble-mediated exchange have been developed in oceans (Asher & Wanninkhof, 1998; Woolf et al., 2007). However, the physical drivers of  $k$  in oceans differ from those in running waters, for example, through the absence of bed-shear (Alin et al., 2011) and hence the applicability of these models to running waters remains unclear. Overall, the contribution of bubbles to  $k$  in running waters remains poorly resolved, and quantifying bubble contributions represents a key challenge for accurate predictions of stream-atmosphere gas fluxes (Hall & Ulseth, 2019; Ulseth et al., 2019).

The  $k$  in running waters can be estimated by methods such as mass balances of tracer gases, floating chambers, the eddy covariance technique, time series analysis of oxygen concentrations, and empirical equations representing channel hydraulics (Hall & Ulseth, 2019). In the widely used mass balance approach,  $k$  is derived from the downstream decline in tracer gas concentrations along a predefined stream reach (Vautier et al., 2020; Wallin et al., 2011; Wanninkhof et al., 1990). This approach is particularly suitable to integrate highly heterogeneous flow conditions present in mountain streams. Hence, the mass balance approach is the only one among the range of existing methods that can potentially yield accurate  $k$  values in mountain streams (Hall & Ulseth, 2019). However, the approach relies on specific tracer gases that are almost exclusively *not* the gas of biogeochemical interest. Ideally, tracer gases remain unaltered by biogeochemical processes during transport, and hence commonly used tracers are biogeochemically inert gases such as propane or sulfur hexafluoride. In turn, this necessitates conversion of  $k$  for the gas of interest

To convert  $k$  between different gases, *Schmidt-number scaling* is commonly applied. Here, the ratio of  $k$  of different gases is assumed to scale with the ratio of the respective Schmidt numbers  $Sc$ , according to  $\frac{k_{gas1}}{k_{gas2}} = \left(\frac{Sc_{gas1}}{Sc_{gas2}}\right)^{-0.5}$ , where  $Sc = \nu/D$ ,  $\nu$  is kinematic viscosity and  $D$  is mass diffusivity (Jähne et al., 1987). It should be noted that this conversion is only valid for gas exchange across the free water surface. In the presence of bubbles, a gas exchange may depend not only on gas diffusivity (represented by the Schmidt number scaling) but also on gas solubility (Hall & Ulseth, 2019). Whereas for some gases of biogeochemical interest, tracer gases with approximately similar diffusivity and solubility exist (see for example the use of Argon to represent Oxygen; Hall & Madinger, 2018), no such complementary gases have been found for CO<sub>2</sub> and CH<sub>4</sub>, the two most relevant GHGs emitted from many streams and rivers.

Several recent developments provide the basis for more accurate quantification of  $k$  in bubbly flow. Multi-gas tracer approaches allow joint estimation of  $k$  for a variety of gases with different diffusivity and solubility under the same field conditions (Asher & Wanninkhof, 1998; Cirpka et al., 1993; Krall et al., 2019). A promising recent development includes membrane inlet mass spectroscopy (MIMS), allowing real-time simultaneous measurement of concentrations of different gases at high frequency (Chatton et al., 2017; Weber et al., 2019). MIMS has been successfully used to quantify  $k$  for helium in streams (Vautier et al., 2020), but its full potential for multi-gas approaches remains to be explored. Another promising new technique to estimate  $k$  in bubbly streams and to gain insights into the driving mechanisms relies on the spectral analysis of ambient sound measurements (Klaus et al., 2019). This method is based on the assumption that both  $k$  and the sound of flowing water are mainly driven by turbulence and bubbles. Klaus et al. (2019) showed that sound pressure levels generally increased with  $k$ , and these increases were strongest at frequencies associated with turbulence and bubbles. These emerging methods call for (a) evaluations of mechanistic  $k$  models using simultaneous multi-tracer mass balance experiments, (b) evaluations of the validity of Schmidt number scaling in bubbly flow, and (c) the development of approaches that

can explicitly target turbulence and bubble contributions and distinguish gas exchange across the free surface from gas exchange through bubbles.

In this study, we thus aimed to evaluate the mechanisms and drivers of  $k$  in running waters under controlled field conditions. Specifically, we performed flume experiments with a wide range of flow conditions to disentangle the effects of turbulence and artificially added bubbles on  $k$ . We inferred  $k$  from evasion experiments with multi-tracer mass balances and compared these data with predictions from mechanistic  $k$  models. We also used the models to separate  $k$  into the free surface- and bubble-mediated gas exchange. Finally, we evaluated the use of ambient sound measurements as proxy measures of the predominant mechanisms that drive  $k$ . We expected that  $k$  would increase with increasing turbulence and bubble flux and that this response can be well predicted by existing mechanistic  $k$  models. We further expected that turbulence and bubble flux would correlate with sound pressure levels at characteristic spectral bands.

## 2. Material and Methods

### 2.1. Experimental Setup

The experiment was carried out in a flume facility located in lower Austria (47°15' N, 15°04' E). The flumes are 40 m long, 0.4 m wide, and 0.4 m high and fed with natural stream water of the nearby *Oberer Seebach*, a nutrient poor third-order subalpine gravel stream that drains a pristine calcareous 20 km<sup>2</sup> catchment with elevations ranging from 600 to 1,878 m above sea level. For more information on the stream and flume facility, see Peter et al. (2014) and Harjung et al. (2019). During the experiment (22–24 August 2019, 9 a.m.–5 p.m.), water and air temperatures ranged between 10–14°C and 20–32°C, respectively. There was no precipitation, winds were low (gust <7 m s<sup>-1</sup>) and the sky was mostly clear (0%–30% cloudiness).

We performed 19 experimental runs in three flumes to simulate a wide range of flow and bubble conditions. The experimental setup is shown in Figure 1; experimental conditions are listed in Table 1. We created bubbles artificially by adding ambient air through a linear air diffuser (Bubble Tubing®) installed at the bottom of the flume (Figure 1b, for details, see Text S1 in Supporting Information S1). This system simplifies the bubble creation process relative to natural streams, where bubbles are entrained at the water surface. Specifically, the bubbles rise more regularly, interact less with other bubbles and spend less time in the water column (Video S1). These distinctions, however, do not bias our experiment because we explicitly account for bubble life time in our modeling approach. Importantly, the experimental setup allowed us to manipulate the bubble flux as a key parameter influencing  $k$ , and to guarantee controlled conditions under which bubble-induced gas exchange can be modeled (see Section 3).

In each flume (F1, F2, and F3), we performed six experimental runs with two different discharge levels of  $Q1 = 3 \text{ L s}^{-1}$  and  $Q2 = 5 \text{ L s}^{-1}$  (F1, F2) and  $Q2 = 5 \text{ L s}^{-1}$  and  $Q3 = 7 \text{ L s}^{-1}$  (F3), and three different bubble flux levels characterized by superficial gas velocities of  $U0 = 0 \text{ m d}^{-1}$ ,  $U2 = 25 \text{ m d}^{-1}$  and  $U3 = 47 \text{ m d}^{-1}$ . For one experimental setting (F2, Q1), we added another bubble flux level of  $U1 = 13.2 \text{ m d}^{-1}$ . Yet given that a constant flow rate was difficult to maintain at such low flow, we limited  $U1$  to only one experimental run. In flume F1 the bottom was covered with black ethylene propylene diene monomer foil only, while in F2 and F3 a layer of ~2 cm of fluvial gravel was added. The gravel had mean ( $\pm$ SD) minimum and maximum axis lengths of  $13 \pm 5.0 \text{ mm}$  and  $32.9 \pm 8.7 \text{ mm}$  ( $n = 100$ ) to resemble conditions typical for pre-alpine streams. Channel slope was  $0.0005 \text{ m m}^{-1}$  (F1, F2) and  $0.0025 \text{ m m}^{-1}$  (F3).

### 2.2. Hydraulic Measurements

We measured water depth ( $d$ ) at 24 locations per flume using a ruler. We further estimated the volumetric bubble flux at nine locations per flume from the air volume captured per unit time by water-filled transparent boxes ( $125 \times 50 \times 35 \text{ mm}^3$ ) placed underwater on top of the aeration system. We quantified water discharge using bucket measurements at the outlet, salt slug injections, and constant rate salt injections as described in detail in Vingiani et al. (2021). We calculated travel time ( $\tau$ ) as the interval between the time points when 50% of the salt slug had passed electrical conductivity loggers placed 5 m below the flume inlet and at the outlet. We also computed the

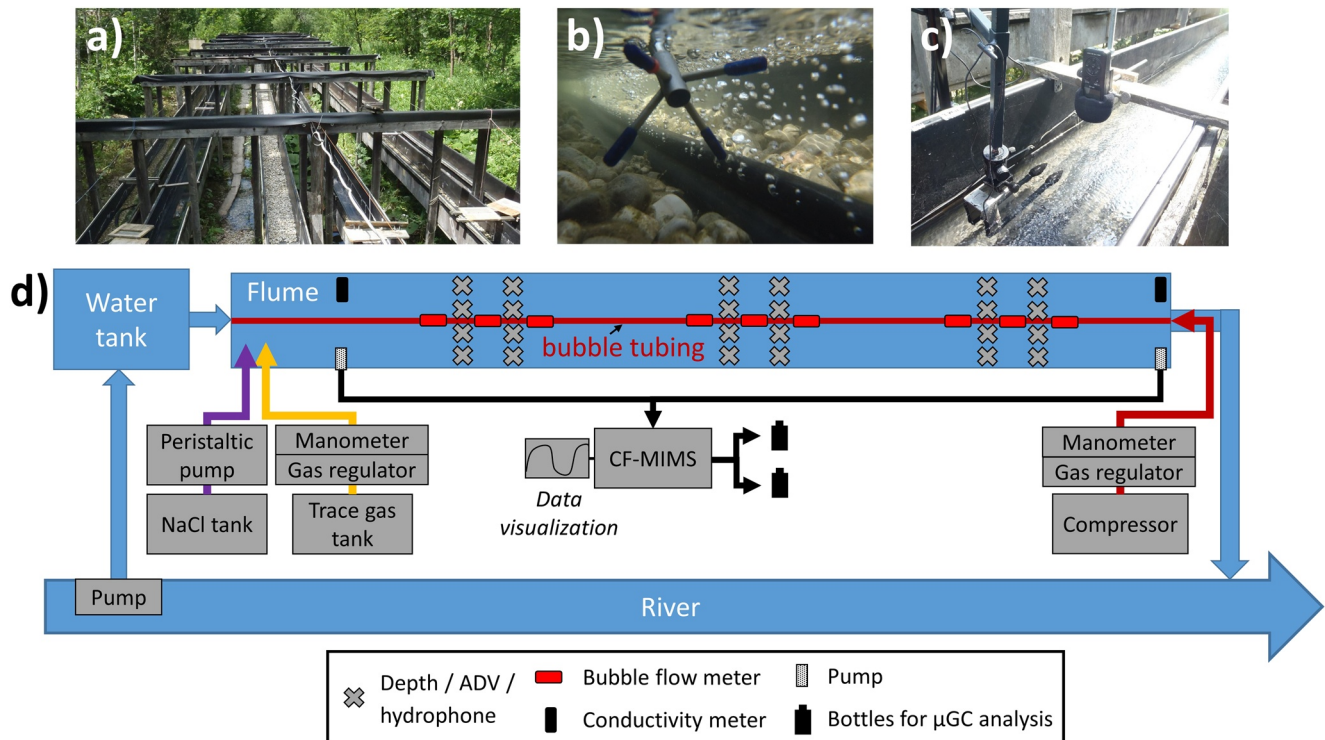


**Figure 1.** Experimental setup and instrumentation. (a) Overview of the flumes, (b) Acoustic Doppler Velocity meter, (c) microphone and hydrophone, (d) sketch of the experimental setup for one of the flumes. River water is pumped through a header tank. Trace gas and a salt solution (NaCl) are continuously injected below the flume inlet and detected by continuous flow membrane-introduction mass spectrometry (CF-MIMS) and conductivity loggers at the upper and low end of the flume. Air bubbles were injected by a linear air diffuser (Bubble Tubing®) (see also b) with air provided by a compressor.

cross-section average flow velocity ( $u$ ) as the distance between the inlet and outlet loggers (35 m) divided by travel time.

We performed Acoustic Doppler Velocity meter measurements using a 4-D down-looking probe (Nortek Vectrino+, Nortek AS, Rud, Norway). We measured longitudinal, lateral, and vertical flow velocities at 200 Hz for 60 s at 24 locations at 5 cm below the water surface (~40–80% of the water column depth) and at horizontal distances of 7 and 12 cm from the channel walls (Figure 1). We estimated the turbulent kinetic energy dissipation rate ( $\epsilon$ ) from spectral fitting on flow velocity spectra using the inertial subrange method. Here, we strictly followed the methodology described by Vingiani et al. (2021) with one exception: in F1 with U0, we removed high-frequency spectral noise prior to spectral fitting using a low-pass first-order Butterworth filter with a cut-off frequency of 10 Hz. We applied a range of standard quality checks on the velocity spectra and  $\epsilon$  estimates, further detailed in Vingiani et al. (2021). Given that  $k$  is related to near-surface turbulence, we standardized all depth-specific empirical  $\epsilon$  estimates to approximate conditions near the water surface (see Text S2 in Supporting Information S1 for details). We propagated errors in  $\epsilon$  estimates resulting from uncertainties in spectral fitting and from spatial variation within the flume. For each  $\epsilon$  estimate, we generated 10,000 bootstrap estimates by sampling from a normal distribution defined by the mean and SD in  $\epsilon$  that resulted from spectral fitting (Vingiani et al., 2021). The population of bootstrapped samples was approximately normally distributed and we, therefore, summarized it using the arithmetic mean  $\pm$  SD.

### 2.3. Ambient Sound Measurements

We used ambient sound measurements as proxies of turbulence and bubble flux and for estimation of bubble radius distributions. We recorded underwater sound largely following the methodology described by Klaus et al. (2019). We captured 35 s long audio signals (1 Hz–22 KHz) at the same locations as the ADV measurements, using two calibrated omnidirectional low flow noise hydrophones (BII-7016, Benthowave Instrument,

**Table 1**  
*Hydraulic Conditions During the Experimental Runs*

Flume	Slope (m m <sup>-1</sup> )	Bed surface	Discharge level	$Q$ (L s <sup>-1</sup> )	Bubble flux level	$U$ (m d <sup>-1</sup> )	$d$ (m)	$u$ (m s <sup>-1</sup> )	$\tau$ (s)
F1	0.0005	foil	Q1	2.6	U0	0.0	0.113	0.063	558
					U2	23.4	0.127	0.060	586
					U3	42.7	0.126	0.060	583
F1	0.0005	foil	Q2	5.3	U0	0.0	0.141	0.111	315
					U2	23.5	0.151	0.108	323
					U3	43.7	0.149	0.109	322
F2	0.0005	foil + gravel	Q1	2.7	U0	0.0	0.080	0.083	421
					U1	13.2	0.080	0.083	421
					U2	26.4	0.083	0.081	430
					U3	50.7	0.083	0.081	429
F2	0.0005	foil + gravel	Q2	5.3	U0	0.0	0.100	0.126	278
					U2	26.0	0.106	0.123	284
					U3	48.8	0.103	0.124	281
F3	0.0025	foil + gravel	Q2	5.1	U0	0.0	0.069	0.202	173
					U2	26.3	0.066	0.207	169
					U3	48.0	0.066	0.207	169
F3	0.0025	foil + gravel	Q3	7.0	U0	0.0	0.077	0.261	134
					U2	25.5	0.083	0.252	139
					U3	47.6	0.083	0.251	139

*Note.*  $S$  is slope,  $Q$  is discharge,  $U$  is superficial gas velocity,  $d$  is water depth,  $u$  is cross-section average flow velocity,  $\tau$  is travel time. Note, that for U0,  $u$  is measured based on salt slug injections and for U1, U2, and U3,  $u$  is computed from flow velocity at U0 and the ratio of the respective measured water depths using the Manning equation.

Collingwood, Ontario, Canada). We mounted the hydrophones at 3 cm free distance to each other on a stainless steel structure fixed on a tripod designed to disturb the flow field as little as possible. We connected the hydrophones to a preamplifier with 26 dB flat gain and a 30 Hz high-pass filter (BII-1006 T1, Benthowave Instrument), sampled the audio signals at a frequency of 44.1 KHz, and stored them on a recorder (DR-100 II, Tascam, Montebello, CA, U.S.A.). We also captured audio signals (2 Hz–22 KHz) at 30 cm above the flume bottom using stereo microphones (Tascam DR-5). Hydrophone and microphone signals did not show any drift when checked against a 1 KHz 94 dB reference SPL (Sound Level Calibrator Model 4230, Bruel & Kær A/S, Nærum, Denmark), before and after the experiment. We minimized flume-related background noise by acoustic dampening of the inflow and outflow using foams, plastic nets, and diffuser stones; hydrophone mounts were physically disconnected from the flume.

We computed the power spectral density ( $PSD$ ) of audio records by means of short-term Fourier transform using the *meanspec* function of the R package *seewave* (Sueur et al., 2008). We segmented audio signals using Hanning windows of 0.37s with 50% overlap. To avoid potential disturbance from handling the recorder, we excluded the first and last second of audio records or any part of the sequence that showed pronounced spikes in visually inspected oscillograms. We normalized the  $PSD$  from microphone recordings to a standard distance to the water surface of 0.1 m, assuming a halving of the sound pressure with a doubling of the distance. As potential correlates of  $\varepsilon$  and  $U$ , we computed the power of the sound signal in a given frequency interval defined as the root-mean-square pressure,  $\rho_{rms} = 2 \int_{\omega_{min}}^{\omega_{max}} PSD(\omega)$ , where  $\omega_{min}$  and  $\omega_{max}$  are the lower and upper limit of the frequency interval (Geay et al., 2017). We chose the interval of 10–100 Hz for the sound generated by turbulence,  $\rho_{rms,t}$  (Geay et al., 2017). We excluded the interval of 44–57 Hz because it was dominated by background noise. We chose the interval of 5–10 kHz for the sound generated by the bursts of surfacing bubbles,  $\rho_{rms,b}$  (see results). Finally, we estimated the bubble radius distributions from underwater sound spectra following Loewen and Melville (1991)

and the average bubble radius following Pandit et al. (1992). The computations and assumptions of this method are provided in Text S3 in Supporting Information S1.

## 2.4. Estimation of $k$

We performed evasion experiments and quantified the evasion rate of tracer gases as the change in their molar concentrations during flume passage using a mass balance approach. We compared the concentrations of helium (He), argon (Ar), xenon (Xe), and methane (CH<sub>4</sub>) between two sampling locations, one at 5 m downstream of the inlet and one at the outlet (Figure 1). We chose these tracer gases because they cover a wide range in diffusivity and solubility and hence affinity to strip into bubbles (Woolf et al., 2007) and are biogeochemically inert (He, Ar and Xe). We assumed that biogeochemical transformation of CH<sub>4</sub> was negligible during flume passage relative to air-water gas exchange, and minimized this risk by removing any sediment or biofilm from the flumes prior to the experiment (for validation of this assumption, see Text S4 in Supporting Information S1). To increase background concentrations and hence the measurement signal, we artificially injected He (all experiments) and Ar and Xe (U2 and U3) 1 m below the flume inlets. We measured gas concentrations using continuous flow membrane-introduction mass spectrometry (CF-MIMS). Details on the gas sampling and analysis procedure are given in Text S5 in Supporting Information S1.

We calculated  $k$  for each gas as  $k = \frac{d}{\tau \cdot 86400} \ln \frac{C_{in} - C_{eq}}{C_{out} - C_{eq}}$ , where  $d$  is water depth (m),  $\tau$  is flume water travel time (s),  $C_{in}$  and  $C_{out}$  are the molar gas concentrations (mol L<sup>-1</sup>) near the in- and outlet water,  $C_{eq}$  is the measured air-equilibrium gas concentration (found negligible for He and Xe), and 86,400 is conversion from s to days. We provide mean  $\pm$  SD  $k$  estimates based on arithmetic means and propagated standard deviations of gas concentration measurements (see Text S5 in Supporting Information S1 for details).

## 3. Modeling

### 3.1. Evaluation of Mechanistic $k$ Models

We fitted the  $k$  measurements to a range of mechanistic models. We assumed  $k$  to be the sum of velocities due to free-surface exchange ( $k_i$ ) and bubble-mediated exchange ( $k_b$ ) (Merlivat & Memery, 1983)

$$k = k_i + k_b \quad (\text{Eq. 1})$$

The theory of  $k_i$  in turbulent open channel flows relies on the principle that dissolved gases will equilibrate faster with the air when the water surface is renewed more rapidly through the motions of small eddies (Moog & Jirka, 1999). Thus,  $k_i$  is described by the small-eddy model (Lamont & Scott, 1970) as

$$k_i = \gamma(\epsilon v)^{1/4} Sc^{-1/2} \quad (\text{Eq. 2})$$

where  $\gamma$  is a parameter. While the small-eddy model has recently been validated for streams and rivers (Wang et al., 2021), there is, to our knowledge, no model to describe  $k_b$  that has been validated for running waters. In oceanography,  $k_b$  was described by the independent bubble model (Woolf, 1997)

$$k_b = \frac{U}{\alpha} \left[ 1 + \left( \frac{Sc^{1/2}}{g\alpha} \right)^{1/f} \right]^{-f} \quad (\text{Eq. 3})$$

where  $\alpha$  is the Ostwald solubility,  $U = Q_b/A$  is the superficial gas velocity of the bubbles (m d<sup>-1</sup>),  $Q_b$  is the volumetric bubble flux (m<sup>3</sup> d<sup>-1</sup>),  $A$  is the water surface area (m<sup>2</sup>), and  $f$  and  $g$  are parameters. Equation 3 assumes that bubbles exchange gases with the surrounding water independently of each other. This assumption was likely fulfilled in our experiment because the air concentration (void fraction) within  $\pm 1$  cm of the bubble plume was small (<3%, see also Figure 1b) which allows a well-mixed gas concentration in the water throughout the water column (Goddijn-Murphy et al., 2016). We computed  $Sc$  following Wanninkhof (2014) and  $\alpha$  as functions of Bunsen or Henry's law solubility constants following Wanninkhof (2014) and Benson and Krause (1976).

Equation 3 neglects bubble size as a factor controlling  $k_b$ . The contribution of bubbles of radius  $a$  to  $k_b$  is described by Woolf et al. (1993) as

$$k_b(a) = \frac{U}{\alpha} [1 - \exp(-T_*(a))] \quad (\text{Eq. 4})$$

where  $T_* = \frac{T}{T_g}$  is the dimensionless lifetime of gas in the bubble,  $T_g = \frac{a}{3ja}$  is the bubble equilibration time (s),  $j = \left( \left( 1 - \frac{2.89}{\sqrt{Re}} \right) \frac{2Du_b}{\pi a} \right)^{0.5}$  is the gas exchange velocity for a single clean bubble (i.e., without contaminants) for  $Re \geq 10$ ,  $Re = 2u_b a / \nu$  is the Reynolds number,  $T = D_b / u_b$  is the bubble lifetime (s),  $u_b = \sqrt{u_s^2 + u^2} + u_{bw}$  is the approximate rise velocity ( $\text{m s}^{-1}$ ) of bubbles in cross flow (Zhang et al., 2014),  $u_s = \sqrt{2.14 \sigma / (\rho a) + 0.505 g_r a}$  is the bubble rise velocity (slip velocity) for bubbly jets in crossflow and  $a > 0.65 \text{ mm}$  (Zhang et al., 2014),  $u_{bw} = (1880a - 0.29) / 100$  is the bubble-induced water velocity ( $\text{m s}^{-1}$ ) within a bubble plume (Zhang & Zhu, 2013),  $D_b = d / \sin(\tan^{-1}(u_s / u))$  is the bubble travel distance in cross flow (m),  $g_r$  is gravitational acceleration ( $9.81 \text{ m s}^{-2}$ ),  $\sigma = (-0.148\vartheta + 75.84) / 1000$  is the surface tension of the air-water interface ( $\text{N m}^{-1}$ ) fitted to data by Jasper (1972),  $\vartheta$  is water temperature ( $^{\circ}\text{C}$ ), and  $\rho$  is water density ( $\text{Kg m}^{-3}$ ) computed following Chen and Millero (1977).

For  $T_* \ll 1$ , bubbles will surface before equilibrating with the water. In this case, bubble mediated exchange is only dependent on  $Sc$  and not on  $\alpha$ , and hence described by Woolf et al. (1993) as

$$k_b(a) = F(a)T(a)4\pi a^2 j(a) \quad (\text{Eq. 5})$$

where  $F(a) = \frac{N(a)}{At}$  is the number flux of bubbles ( $\text{m}^{-2} \text{ s}^{-1}$ ),  $N$  is the total number of bubbles and  $t$  is time. With the superficial gas velocity  $U(a) = \frac{N(a)V(a)}{At}$  and the bubble volume for a given bubble radius  $V(a) = 4/3\pi a^3$ , we obtain  $F(a) = \frac{U(a)}{4/3\pi a^3}$  and can formulate a mean bubble lifetime model as

$$k_b(a) = \frac{U}{a} 3T(a)j(a)b \quad (\text{Eq. 6})$$

where  $b$  is a dimensionless parameter that accounts for uncertainty in  $j$ , which can vary largely depending on the specific hydrodynamic conditions and bubble-bubble interactions in cross-flow bubble plumes (Kantarci et al., 2005; Memery & Merlivat, 1985; Woolf, 1993). We estimated the total  $k_b$  of the whole bubble population as the sum of the bubble-radius specific  $k_b(a)$  weighted by the volumetric contribution of all bubbles with a specific radius, resulting in the weighted mean bubble lifetime model

$$k_b = \sum [N(a)V(a)k_b(a)] / \sum [N(a)V(a)] \quad (\text{Eq. 7})$$

### 3.2. Model Fitting Procedure

We fitted Equation 2 to data from experiments with no bubble additions and refer hereafter to this model as LS70. We also fitted Equations 3, 6 and 7 to all experimental data after inserting into Equation 1. We refer to these models as W97, W93m, and W93w, respectively, hereafter. We fitted the models using the nonlinear regression function *nls* in R and evaluated the normality and homoscedasticity of model residuals. We also tested if the model W93m would improve fits relative to W97, and if W93w would further improve model fits, using the likelihood ratio test by means of the *lmtest* function of the statistical package *lmtest* (Zeileis & Hothorn, 2002). We estimated uncertainties in model parameters by propagating uncertainties in  $\varepsilon$  and  $k$  estimates using a bootstrap approach. Specifically, we sampled  $\varepsilon$  and  $k$  from log-normal and normal distributions, respectively, defined by the propagated means and SDs of each original estimate. We generated 10,000 bootstrap estimates and report the 2.5%, 50%, and 97.5% quantiles of the resulting distributions of model parameters.

We used each of the four models to calculate the relative contribution of bubble-mediated to total gas exchange velocities  $\left( \frac{k_b}{k_b+k_i} \right)$ . First, we derived bubble contributions from the comparison of measured  $k$  and  $k_i$  modeled using LS70,  $\frac{k_b}{k_b+k_i} = \frac{k_{meas} - k_{i,LS70}}{k_{meas}}$ , assuming that the  $\varepsilon$ - $k_i$  relationship is similar in experiments with and without bubbles. For the other models, we derived bubble contributions from the comparison of  $k_b$  and  $k_i$  modeled using W97, W93m, and W93w, respectively,  $\frac{k_b}{k_b+k_i} = \frac{k_{b,mod}}{k_{b,mod} + k_{i,mod}}$ . In these models, the effect of bubbles on  $\varepsilon$  is explicitly accounted for.

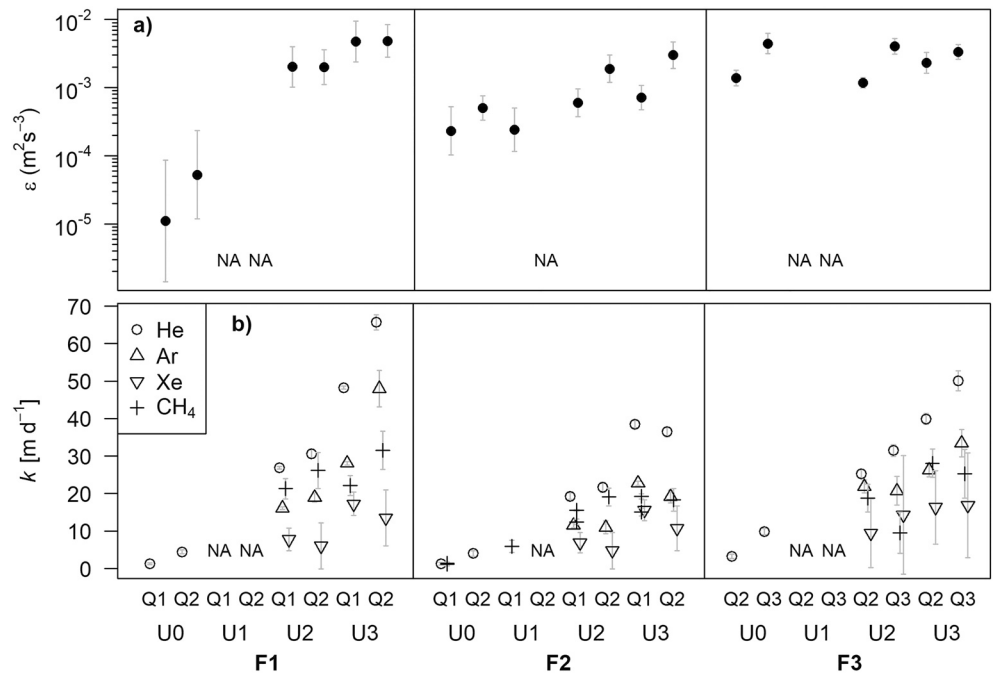


**Figure 2.** Turbulent kinetic energy dissipation rate ( $\epsilon$ , (a)) and gas exchange velocity ( $k$ ) of helium, argon, xenon, and methane (b) in the different flumes (F) for different levels of discharge (Q1–Q3) and superficial gas velocities (U0–U3). Logarithmic error bars in (a) show bootstrapped standard deviations of mean estimates and multiple measurements per flume. Error bars in (b) show propagated standard deviations of gas concentrations measured continuously for 15 min. NA is not available.

## 4. Results

### 4.1. Turbulence and Sound Pressure Characteristics

The flow velocity measurements allowed us to successfully compute  $\epsilon$ , as 84% of all measurements passed all quality checks for  $\epsilon$  estimation. We observed an inertial subrange in longitudinal (u), transversal (v), and vertical (w1, w2) velocity fluctuations for wave numbers of around 100–1,000  $\text{rad m}^{-1}$  (Figure S1 in Supporting Information S1). The median coefficient of determination ( $R^2$ ) of spectral fits that passed all quality checks was 0.58, 0.60, 0.60, and 0.60, respectively (range 0.38–0.73, 0.20–0.76, 0.10–0.74, 0.40–0.74), indicating moderately good fits. The  $\epsilon$  estimates for the different flow directions were always within the 95% confidence intervals of the respective other directions. We, therefore, assume turbulence to be isotropic and report in the following only  $\epsilon$  estimates for the vertical component (w1). The coefficient of variation (CV) of  $\epsilon$  estimates was 1.50, 1.32, 1.07, and 1.09 as a median across all experiments and ranged from 0.41, 0.48, 0.40, and 0.41 in one of the most turbulent experiments (F3, Q3, U0) to 6.15, 4.28, 4.72 and 4.67 in the least turbulent experiment (F1, Q1, U0), respectively.

The underwater sound spectra showed distinct responses to discharge and bubble injections (Figure S2 in Supporting Information S1). In the absence of bubbles, the *PSD* of sound pressure levels decreased between 30 and 200 Hz as a result of background noise and/or partial cancellation of flow-induced pressure fluctuations (Bassett et al., 2014). An increase in discharge leads to an increase in sound pressure in this interval. Bubbles caused a primary *PSD* peak at 250 Hz–2 KHz due to oscillations under water and a secondary peak at 5–10 KHz due to bursting at the water surface. Similar responses to bubbles were apparent in sound spectra above the water surface (Figure S3 in Supporting Information S1).

### 4.2. Response of Turbulence and Gas Exchange Velocities to Treatments

The experiments resulted in  $\epsilon$  ranging from  $10^{-5}$  to  $5 \cdot 10^{-3} \text{ m}^2 \text{ s}^{-3}$  and  $k$  ranging from 1.2 to  $65.7 \text{ m d}^{-1}$  (Figure 2). The  $k$  was highest for He, followed by Ar, CH<sub>4</sub>, and Xe, as it can be expected from the range of Schmidt numbers



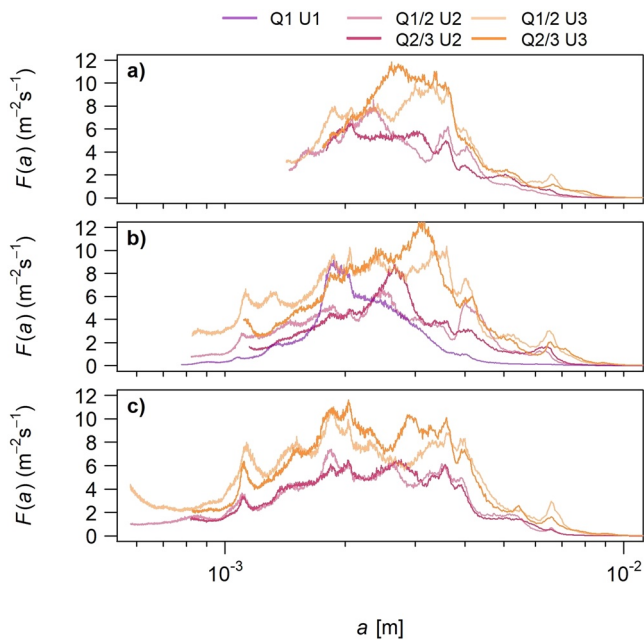


**Figure 3.** Average frequency distribution of the bubble number flux ( $F$ ) per bubble radius ( $a$ ) for the different experimental runs in flume F1 (a), flume F2 (b) and flume F3 (c) for different bubble flux levels ( $U$ ) and discharge levels ( $Q$ ) (Q1 and Q2 in flumes F1 and F2; Q2 and Q3 in flume F3).

and Ostwald solubilities that these gases cover, ranging from around 200 and 0.009, respectively, for He, to 1200 and 0.15, respectively, for Xe (Figure S4 in Supporting Information S1). The CV of  $k$  estimates was 0.13 as a median across all experiments and was generally lowest for He (0.05) and highest for Xe (0.58). Both  $\varepsilon$  and  $k$  responded strongly to discharge and bubble flow treatments and varied between flumes because of their distinct channel slope, bottom roughness, and water depth (Figure 2, Table 1). An increase in discharge resulted generally in an increase in  $\varepsilon$  and  $k$ . Bubbles enhanced  $\varepsilon$  most strongly in F1, in a less pronounced manner in F2 and not at all in F3. Bubbles also enhanced  $k$ , in particular in F1. A doubling in the bubble flux generally further enhanced  $\varepsilon$  and  $k$ . In the absence of bubbles,  $\varepsilon$  was higher in F2 and F3 relative to F1, which is likely due to higher bottom roughness in these flumes. In addition,  $\varepsilon$  and  $k$  were higher in F3 relative to F2 and F1 likely because of the higher channel slope. Overall, the experiments demonstrated a strong response of turbulence and gas exchange to hydraulic conditions.

### 4.3. Bubble Dynamics

The modeled bubble radius ranged from 1 to 7 mm and averaged between 1.9 and 2.9 mm depending on the experiment (Figure 3). This is supported by visual observations from an underwater photograph, indicating bubble radii of around 2 mm (Figure S5 in Supporting Information S1). The bubble radii were within the range guaranteed by the fabricator of the linear air diffuser, and similar to ranges found in staircase chute flows (Chanson & Toombes, 2003). The mean bubble radius increased slightly with discharge and was highest in F1 and lowest in F3 (Table 2). The bubble life time was around 0.20–0.48 s, increased with discharge, and was highest in F1 and lowest in F3 because of the longer travel path in deeper water. Bubble equilibration times were 12–170 s. As a result,  $T_*$  was  $\ll 1$ , indicating that bubbles did not equilibrate with

**Table 2**

*Bubble Characteristics for the Different Experiments, Given as Arithmetic Means ( $\pm SD$ ) of all Measurements per Flume.  $U$  is Superficial Gas Velocity,  $a$  is Bubble Radius,  $F$  is Bubble Number Flux,  $T$  is Bubble Life Time,  $T_g$  is Bubble Equilibration Time and  $T_*$  is Non-dimensional Lifetime of Different Tracer Gases in the Bubbles ( $T/T_g$ )*

Flume	Discharge level	Bubble flux level	$U$ (m d <sup>-1</sup> )	$a$ (mm)	$F$ (s <sup>-1</sup> nozzle <sup>-1</sup> )	$T$ (s)	$T_g$ (s)				$T_*$			
							He	Ar	Xe	CH <sub>4</sub>	He	Ar	Xe	CH <sub>4</sub>
F1	Q1	U2	23.4 ± 8.0	2.6 ± 0.2	7 ± 3	0.40 ± 0.01	143	63	21	64	0.0028	0.0064	0.0194	0.0063
F1	Q2	U2	23.5 ± 7.1	2.8 ± 0.2	6 ± 1	0.48 ± 0.00	163	71	23	72	0.0030	0.0069	0.0209	0.0068
F1	Q1	U3	42.7 ± 8.3	2.7 ± 0.2	10 ± 3	0.40 ± 0.00	155	68	23	70	0.0026	0.0058	0.0177	0.0057
F1	Q2	U3	43.7 ± 8.0	2.9 ± 0.1	9 ± 2	0.48 ± 0.00	170	74	24	76	0.0028	0.0065	0.0196	0.0063
F2	Q1	U1	13.2 ± 5.0	2.1 ± 0.1	8 ± 2	0.24 ± 0.00	NA	NA	NA	46	NA	NA	NA	0.0053
F2	Q1	U2	26.4 ± 7.5	2.2 ± 0.2	10 ± 3	0.25 ± 0.01	113	49	16	50	0.0023	0.0052	0.0159	0.0051
F2	Q2	U2	26.0 ± 8.0	2.5 ± 0.2	8 ± 2	0.33 ± 0.00	134	57	19	58	0.0025	0.0058	0.0179	0.0058
F2	Q1	U3	50.7 ± 15.2	2.1 ± 0.2	19 ± 6	0.25 ± 0.01	107	46	15	47	0.0024	0.0055	0.0166	0.0054
F2	Q2	U3	48.8 ± 14.1	2.5 ± 0.2	14 ± 3	0.33 ± 0.00	132	57	19	58	0.0025	0.0057	0.0175	0.0056
F3	Q2	U2	26.3 ± 5.6	2.0 ± 0.4	13 ± 8	0.20 ± 0.01	89	39	13	40	0.0022	0.0052	0.0157	0.0051
F3	Q3	U2	25.5 ± 5.6	2.1 ± 0.3	11 ± 4	0.26 ± 0.01	95	41	13	42	0.0027	0.0063	0.0192	0.0062
F3	Q2	U3	48.0 ± 9.3	1.9 ± 0.4	24 ± 14	0.20 ± 0.01	81	36	12	36	0.0024	0.0056	0.0168	0.0054
F3	Q3	U3	47.6 ± 8.3	2.2 ± 0.3	19 ± 7	0.26 ± 0.01	97	42	14	43	0.0027	0.0062	0.0189	0.0061

Note. NA is not available.

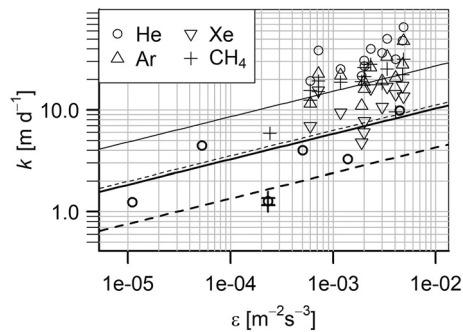


**Figure 4.** Air-water gas exchange velocity ( $k$ ) for helium (He), argon (Ar), xenon (Xe), and methane ( $\text{CH}_4$ ) relative to the turbulent kinetic energy dissipation rate ( $\epsilon$ ). Symbols with thick outlines denote experiments with no bubble additions and symbols with thin outlines denote experiments with bubble additions. The lines denote the  $\epsilon$ - $k$  relationship according to surface-renewal theory (Equation 2) following Moog and Jirka (1999) where  $\gamma = 0.16$  (thick lines) and according to Zappa et al. (2007) where  $\gamma = 0.42$  (thin lines). Lines are exemplarily shown for water temperatures of  $10^\circ\text{C}$  for the most diffusive and least diffusive gases He (solid lines) and Xe (dashed lines), respectively.

the surrounding water. The calculated bubble number flux (Figure 3) ranged from 6 to  $24 \text{ s}^{-1}$  when expressed per nozzle (Table 2). For F2, Q2, and U3, a flux of  $14 \text{ s}^{-1} \text{ nozzle}^{-1}$  would imply that five bubbles were released within the average bubble life time of 0.33 s. The underwater photograph confirms this prediction and provides a rough validation of our bubble flux estimates (Figure S5 in Supporting Information S1).

#### 4.4. Evaluation of $k$ Models

In general,  $k$  increased with  $\epsilon$  following surface renewal theory (Figure 4). Observations from experiments without bubble additions followed roughly predictions by Moog and Jirka (1999) where  $\gamma = 0.16$  in Equation 2. During bubble additions,  $k$  values were higher than predictions by Zappa et al. (2007) where  $\gamma = 0.42$ . These predictions constitute rather high estimates for free-surface exchange (Wang et al., 2015), which indicates that gas is exchanged not only through the free surface but also through bubbles.

When fitting  $k$  models to our data, the parameter  $\gamma$  varied from 0.15 to 0.21 and was significant in all models ( $p < 0.05$ ), except W93w ( $p = 0.058$ ; Table 3). The parameter was similar among all models, given the 95% confidence intervals ranging from 0.07 to 0.22 to 0.13–0.30. The parameters specific to the W97 model were  $f = 1.45$  and  $g = 12.32$ , but only  $g$  was significant because of the wide confidence interval in  $f$  (0.69–2.34). In the bubble-size specific models, parameter  $b$  was significant and amounted to 2.99 and 4.71, respectively.

All  $k$  models fitted the data well. The good fit was indicated by linear regressions of observed versus predicted values with insignificant intercepts, slopes close to 1 (given their 95% confidence intervals), and  $R^2$  values of 0.72–0.83 (Figure 5, Table S1 in Supporting Information S1). Accounting for average bubble size through model W93m improved model fits relative to the description by model W97 ( $R^2$  of 0.806 vs. 0.773; likelihood ratio test, log-likelihood  $-196.29$  vs.  $-191.67$ ,  $\chi^2 = 9.23$ ,  $p = 0.002$ ). Accounting for bubble-specific size distributions (W93w) instead of assuming an average bubble size (W93m) improved the model further ( $R^2$  of 0.830 vs. 0.806; likelihood ratio test, log-likelihood  $-191.67$  vs.  $-187.74$ ,  $\chi^2 = 7.87$ ,  $p < 0.001$ ).

**Table 3**  
Parameterization of Different  $k$  Models

Model	Parameter	Estimate				df
		Mean	SD	$t$	$p$	
LS70 <sup>a</sup>	$\gamma$	0.15 (0.12; 0.18)	0.02 (0.01; 0.04)	6.28 (4.08; 10.75)	0.0002 (0.0000; 0.0036)	8
W97	$\gamma$	0.21 (0.13; 0.30)	0.08 (0.06; 0.10)	2.72 (1.55; 4.05)	0.0086 (0.0002; 0.1256)	57
	$f$	1.45 (0.69; 2.34)	0.94 (0.75; 3.25)	1.63 (0.21; 2.48)	0.1084 (0.0161; 0.8340)	
	$g$	12.32 (10.50; 16.20)	2.46 (1.36; 7.29)	4.95 (2.15; 8.59)	0.0000 (0.0000; 0.0361)	
W93 m	$\gamma$	0.17 (0.09; 0.25)	0.08 (0.06; 0.10)	2.22 (1.12; 3.45)	0.0301 (0.0011; 0.2685)	58
	$b$	2.99 (2.64; 3.29)	0.31 (0.25; 0.40)	9.52 (7.18; 12.05)	0.0000 (0.0000; 0.0000)	
W93w	$\gamma$	0.14 (0.07; 0.22)	0.07 (0.06; 0.09)	1.93 (0.89; 3.02)	0.0581 (0.0038; 0.3781)	58
	$b$	4.71 (4.24; 5.16)	0.45 (0.36; 0.58)	10.39 (7.76; 13.35)	0.0000 (0.0000; 0.0000)	

Note. Given are bootstrapped medians and 95% confidence intervals.  $t$  is  $t$  values,  $p$  is  $p$  values, df is degrees of freedom.

<sup>a</sup>Fitted to conditions without bubble additions only.

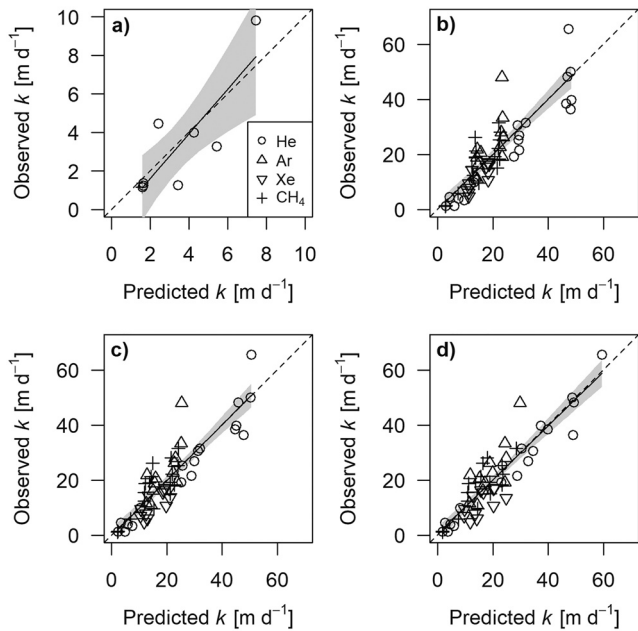


**Figure 5.** Observed versus predicted gas exchange velocity ( $k$ ) for the models LS70 (a), W97 (b), W93m (c), W93w (d). The dashed line is the 1:1 line. The solid line is the linear regression. For regression equations, see Table S1 in Supporting Information S1. The gray shading denotes 95% confidence intervals of the regression line. None of the regression intercepts is significantly different from 0 and none of the slopes is significantly different from 1.

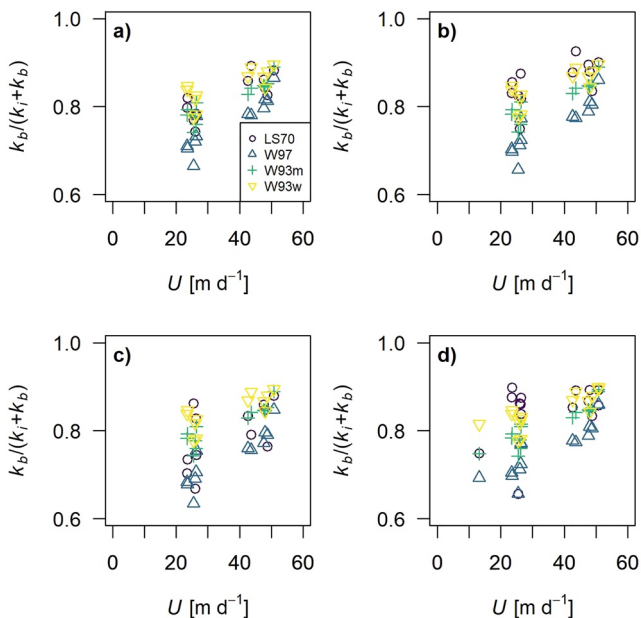


**Figure 6.** Relative contribution of bubble-mediated to total gas exchange velocity ( $k_b / (k_i + k_b)$ ) according to the models LS70, W97, W93m, and W93w, for helium (a), argon (b), xenon (c), and methane (d) for experiments with bubble injections. Shown are bootstrap median values. The 95% confidence intervals around these medians are  $(-0.06, +0.11)$  (LS70),  $(-0.13, +0.11)$  (W97),  $(-0.12, +0.10)$  (W93m), and  $(-0.11, +0.08)$  (W93w) as medians across all observations.

#### 4.5. Modeled Contribution of Bubbles to Gas Exchange Velocities

The bubble-mediated gas exchange was the dominant gas exchange pathway in all experiments with bubble injections. Bubbles contributed to 66–93%, 64–87%, 74–89%, and 78–90% to total  $k$  values according to the models LS70, W97, W93m, and W93w, respectively (Figure 6). The 95% confidence intervals around these means were around  $\pm 10\%$ . The bubble contribution increased with  $U$  but was independent of the tracer gas.

#### 4.6. A Sound Parameterization of $\varepsilon$ and $U$

The key variables of the evaluated  $k$  models,  $\varepsilon$  and  $U$ , correlated with sound pressure levels at characteristic spectral frequencies. The  $\varepsilon$  increased significantly with  $\rho_{rms,t}$  in experiments without bubbles ( $R^2 = 0.90$ , Figure 7a, Table S2 in Supporting Information S1). Under the presence of bubbles,  $\rho_{rms,t}$  increased further, while  $\varepsilon$  did not. In bubble experiments,  $\rho_{rms,b}$  increased significantly with  $U$ , both for sound below the water surface ( $R^2 = 0.90$ , Figure 7b) and above ( $R^2 = 0.76$ , Figure 7c).

### 5. Discussion

#### 5.1. The Value of Mechanistic Models in Stream Gas Exchange Research

We combined experiments and mechanistic modeling to unravel the quantity and pathways of gas exchange in running waters. We showed that mechanistic  $k$  models, although originally developed in oceans, provide accurate predictions in open channel flow, once they are suitably calibrated. An important strength of the tested models is that they allow predictions of  $k$  for any sparingly soluble gas, while many other field methods and empirical models are limited to specific gases and may require conversion of  $k$  to other gases of interest. In particular, the tested models overcome the problem of Schmidt number scaling to yield potentially inaccurate  $k$  values in bubbly flow (Hall & Madinger, 2018). The mechanistic  $k$  models also advance the theoretical understanding of gas exchange pathways. For example, the evaluated models can be explicitly used to test the recent hypothesis by Ulseth et al. (2019) that high  $k$  values in mountain streams are primarily driven by bubble-mediated rather than free surface exchange. Understanding the source mechanisms of  $k$  is particularly important for accurate quantification of high GHG emissions from mountain streams and their response to global change (Horgby et al., 2019).

#### 5.2. Are Air–Water Gas Exchange Processes Universal?

The findings from this study are likely relevant for many streams and rivers and suggest similarities but also differences in gas exchange processes between running and standing waters. First of all, turbulent kinetic energy dissipation rates ( $\varepsilon$ ) and  $k$  in our flume experiments covered a large portion of the range found in running waters worldwide (cf. Ulseth et al., 2019). Furthermore, the estimated bubble size distributions likely resembled natural conditions in stream cascades as suggested by striking similarities in sound spectra with peaks around 0.25–2 KHz (Klaus et al., 2019). As a result, the modeled bubble contribution to  $k$  in our flumes had a similar range as

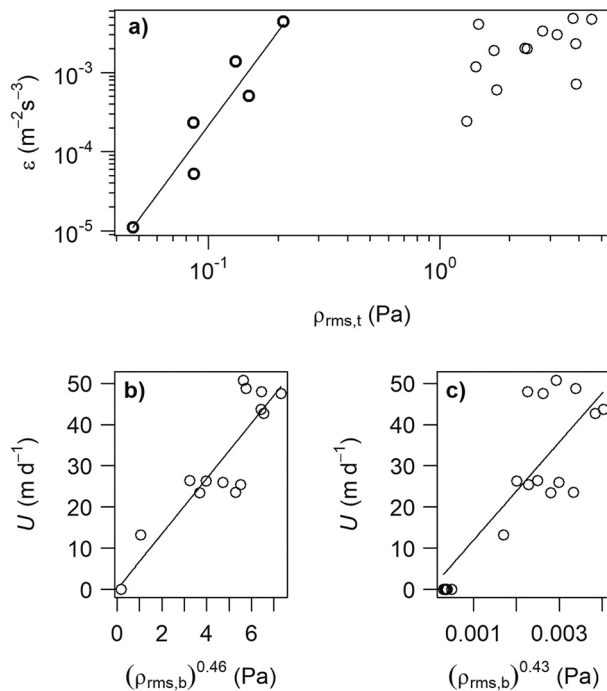


**Figure 7.** Relationship between indicators of underwater sound, turbulence and bubble flux. (a) root-mean-square sound pressure at 10–100 kHz ( $\rho_{rms,t}$ ) versus turbulent kinetic energy dissipation rate ( $\epsilon$ ), (b) root-mean-square sound pressure at 5–10 kHz measured underwater ( $\rho_{rms,b}$ ) versus superficial gas velocity ( $U$ ), (c) as in (b) but for sound measured above the water surface. Lines show best fits of regression models: (a)  $\log_{10}(\epsilon) = 3.83 \log_{10}(\rho_{rms,t}) + 0.46$  (fitted to data without bubbles only; circles with thick outline), (b)  $U = 6.73 \rho_{rms,b}^{0.46}$ ; (c)  $U = 1.19 \cdot 10^4 \rho_{rms,b}^{0.43}$ . For model details, see Table S2 in Supporting Information S1.

previously reported for river cascades (Cirpka et al., 1993) and breaking ocean waves (Deike & Melville, 2018).

Even though the tested  $k$  models were originally developed in standing waters, our model parameterizations were generally within the range of literature values from lake and ocean research. The parameter  $\gamma$  that relates  $k$  to  $\epsilon$  was similar to another flume experiment (Moog & Jirka, 1999), and at the lower end of values previously reported for standing waters (Tokoro et al., 2008; Vachon et al., 2010; Wang et al., 2015; Zappa et al., 2007). The parameters  $f$  and  $g$  that describe bubble-mediated exchange in the model W97 were strikingly similar to parameters given by Woolf (1997) for gas exchange in ocean breaking waves. On the other hand, parameter  $b$  in the models W93m and W93w was  $>1$ , indicating that these models underestimated bubble-mediated gas exchange in our experiment. A likely explanation for this mismatch is that we underestimated the bubble-specific gas exchange velocity  $j$  or the bubble life time  $T$  (Equation 6). In fact,  $j$  and  $T$  can vary by up to a factor of 10, depending on the model and the assumptions about the specific bubble characteristics (Memery & Merlivat, 1985; Woolf, 1993). Here, an important role is played by surfactants. Surfactants slow down the gas exchange, but also the bubble rise velocity and therefore have a counteracting effect on  $j$  and  $T$ . Which of these effects dominated in our experiment or whether other, undescribed dynamics of bubble clouds in cross-flow played a role is beyond the scope of this paper. However, the overall similarities and differences in model parameters between our experiment and previous studies highlight the potential for exciting avenues for further research on how universal gas exchange processes are across various aquatic systems.

### 5.3. Scaling of $k$ Among Gases in Bubbly Streams

The mechanistic  $k$  models provide a means for accurate scaling of  $k$  for a given set of gases and water temperatures. The  $k$  of a given gas and temperature can be scaled to another gas or temperature by multiplying it with the ratio of the corresponding  $k$  values calculated by Equation 1–4. Whether such

an approach is required instead of the traditional Schmidt number scaling depends on the bubble equilibration and life times, and hence  $T_*$ . In our experiment,  $T_*$  was  $\ll 1$ , indicating that the bubbles did not equilibrate with the surrounding water for the measured gases. In this case, both free-surface and bubble-mediated gas exchange scales with  $Sc^{-0.5}$  (Woolf, 1993). As a result, Schmidt number scaling provided accurate  $k$  values in our experiment (Figure S6 in Supporting Information S1) and the estimated bubble contribution to  $k$  was similar for gases of widely different  $Sc$  (Figure 6). However, Schmidt number scaling would have failed if  $T_*$  reached values near one or higher. Such conditions are theoretically met for  $CO_2$  exchange and water depths of 0.3–0.5 m (Figure S7 in Supporting Information S1). Bubble intrusion depths of this magnitude are plausible in natural streams, for example, through waterfalls (Lakso, 1988). The deeper and faster a stream, the higher  $T_*$  will theoretically be (Figure S7 in Supporting Information S1) and the more will Schmidt number scaling lead to erroneous  $k$  estimates. We thus propose that future studies need to evaluate  $T_*$  for given stream flow conditions in order to choose the appropriate method to scale  $k$  among gases.

### 5.4. Estimating $k$ Using Ambient Sound Measurements

Our findings highlight the potential of ambient sound measurements for estimating key drivers of gas exchange, including  $\epsilon$ ,  $U$ , and bubble size distributions. The great strength of sound measurements is that they allow estimates of several relevant measures through a single instrument, saving time and resources. Our findings provide a mechanistic underpinning of the previously reported correlations between  $k$  and ambient sound signatures (Klaus et al., 2019; Morse et al., 2007). Our findings also corroborate previous reports on correlations between turbulence

and sound spectral metrics resulting from pressure fluctuations due to the interaction between water flow and hydrophone (Bassett et al., 2014). Further, we provide novel correlations between sound spectral signatures and  $U$  based on the mechanism that with increasing  $U$ , more bubbles will surface per unit time and collectively emit more sound. Finally, we stress the potential of hydrophones to provide estimates on bubble size distributions. Such estimates are currently rare in natural running waters (but see Leighton and Walton (1987)) and are usually limited to idealized hydraulic conditions in artificial channels (Chanson, 1995; Chanson & Toombes, 2003). Because of their relative ease to use, microphones and hydrophones may be particularly useful in applications where evaluations of bubble contributions to  $k$  are needed across many sites. More rigorous investigations of bubble dynamics in natural streams and rivers may lead to a similar breakthrough in understanding gas exchange mechanisms, as it has in oceanography (Deane & Stokes, 2002).

### 5.5. Study Limitations and Challenges for Future Work

Several conditions in our flume experiment may differ from natural field conditions and may have affected our results. *First*, in absence of bubbles, we may have overestimated near-surface  $\varepsilon$  when extrapolating  $\varepsilon$  from deeper measurements. This could explain the relatively low estimate of the model parameter  $\gamma$  in our experiment. Difficulties in scaling  $\varepsilon$  across depth encompass a general problem in shallow running waters where turbulence increases with depth and proximity to the channel bed (Nezu & Nakagawa, 1993). *Second*, in presence of bubbles, we may have underestimated  $\varepsilon$ , because we were not able to estimate  $\varepsilon$  within the center of the bubble plume. This is supported by the fact that our  $\varepsilon$  values were relatively low for given levels of  $k$  (Figure 4) and below the threshold level ( $\varepsilon = 0.02 \text{ m}^2 \text{ s}^{-3}$ ) that is needed for bubble entrainment in natural streams (Ulseth et al., 2019). Errors in  $\varepsilon$  would primarily propagate into errors in  $\gamma$ , but less into errors in other model parameters or bubble contributions (Text S7 in Supporting Information S1). *Third*, despite large efforts to reduce background noise in our flume facility, residual noise may have affected the relationship between sound pressure signatures and  $\varepsilon$  and  $U$ . For example, the disproportional increase of  $\rho_{rms,t}$  relative to  $\varepsilon$  in bubble experiments is likely due to sound created during bubble release from the nozzles of the linear aeration system (Deane & Czerski, 2008; Miao et al., 2018). *Fourth*, the clear spectral separation between the sounds of surfacing and rising bubbles in our experiment may not always be present under field conditions (Klaus et al., 2019). *Fifth*, our linear air diffuser created homogeneous plumes with well-separated bubbles. In natural streams, bubbles may occur in dense clouds and interact in complex ways with each other, with consequences for the emitted sound (Yoon et al., 1991) and gas exchange (Woolf et al., 2007, see also Movie S1). To further investigate and overcome these limitations, future studies should develop methods to accurately estimate turbulence just below the water surface and within bubble plumes and evaluate relationships between sound signatures, turbulence, bubbles, and gas exchange under natural conditions across stream networks.

Our  $k$  model parameters had relatively large uncertainty (CI of up to a factor of 2 or more) and this was mainly attributed to uncertainty in  $\varepsilon$  (median CV = 127%). Uncertainty in  $\varepsilon$  was mainly due to high spatial variability between measurement sites and relatively low signal-to-noise ratios causing problems in fitting energy dissipation models to flow velocity spectra. The residual uncertainty was mainly due to errors in  $k$  estimates (median CV = 13%) and attributed to temporal variability in measured tracer gas concentrations in flume water. Further reduction in methodological and experimental uncertainties, especially in turbulence estimates, will allow a more rigorous comparison of model parameterizations among studies and systems. Such comparisons open the exciting opportunity to evaluate the universality of scaling relationships of  $k$  across a wide range of aquatic systems including standing and running waters and to identify conditions that modify these relationships (Wang et al., 2015, 2021).

## 6. Conclusions

Based on a flume experiment with integrated bubble plumes, we provide the first parameterizations of mechanistic  $k$  models for running waters that explicitly distinguish between the free surface and bubble-mediated gas exchanges. The models also allow for scaling of  $k$  values among different gases and overcome limitations of traditional Schmidt number scaling in bubbly flow. We also provide a proof-of-concept to derive important input variables to these models from ambient sound measurements. In order to further advance the mechanistic

understanding and quantification of gas exchange rates in bubbly streams and rivers, we recommend two complementary approaches: Multiple-tracer-gas injection experiments will provide detailed and accurate  $k$  estimates for individual stream reaches, while relatively simple ambient sound measurements will provide complementary insights into the physical processes that facilitate gas exchange at higher spatio-temporal resolution and be useful for upscaling.

## Data Availability Statement

All data is provided in Tables included in this manuscript or in the supplementary material. The full data set is also available through the Swedish National Data Service: <https://doi.org/10.5878/j46g-rw37>. Relevant R code for calculation of turbulent kinetic energy dissipation, bubble size distributions, bubble life times and bubble equilibration times is provided under the GPL-3.0 License: <https://doi.org/10.5281/zenodo.5765183> and <https://doi.org/10.5281/zenodo.5765139>.

## Acknowledgments

This study was supported by the Transnational Access grant ExSONIC through the European Commission EU H2020-INFRAIA-project AQUACOSM (Grant No. 731065) and by Lars Hierta Memorial Foundation, both awarded to Marcus Klaus, the European Community's Horizon 2020 Excellent Science Programme (Grant No. H2020-EU.1.1.-770999) awarded to Gianluca Botter, and the project HYDRO-DIVERSITY awarded to Jakob Schelker by the Austrian Academy of Sciences. MIMS and mobile lab were developed through the French CRITEX program (Grant No. ANR-11-EQPX-0011) awarded to Thierry Labasque. We thank Astrid Harjung for help with setting up the flumes, David Vilbert for technical assistance with MIMS, Michael Scharner and Paul Schwaigerlehner for field assistance, Gertraud Steniczka for logistical assistance, Katrin Attermeyer for lab support, and Johann Waringer for providing the ADV.

## References

- Alin, S. R., Rasera, M. D. F. L., Salimon, C. I., Richey, J. E., Holtgrieve, G. W., Krusche, A. V., et al. (2011). Physical controls on carbon dioxide transfer velocity and flux in low-gradient river systems and implications for regional carbon budgets. *Journal of Geophysical Research: Biogeosciences*, *116*(1), G01009. <https://doi.org/10.1029/2010JG001398>
- Asher, E., & Wanninkhof, R. (1998). The effect of bubble-mediated gas transfer on purposeful dual-gaseous tracer experiments. *Journal of Geophysical Research*, *103*(C5), 10555–10560. <https://doi.org/10.1029/98JC00245>
- Bassett, C., Thomson, J., Dahl, P. H., & Polagye, B. (2014). Flow-noise and turbulence in two tidal channels. *Journal of the Acoustical Society of America*, *135*(4), 1764–1774. <https://doi.org/10.1121/1.4867360>
- Benson, B. B., & Krause, D. (1976). Empirical laws for dilute aqueous solutions of nonpolar gases. *The Journal of Chemical Physics*, *64*(2), 689–709. <https://doi.org/10.1063/1.432215>
- Chanson, H. (1995). Air-water gas transfer at hydraulic jump with partially developed inflow. *Water Research*, *29*(10), 2247–2254. [https://doi.org/10.1016/0043-1354\(95\)00056-Q](https://doi.org/10.1016/0043-1354(95)00056-Q)
- Chanson, H., & Toombes, L. (2003). Strong interactions between free-surface aeration and turbulence in an open channel flow. *Experimental Thermal and Fluid Science*, *27*(5), 525–535. [https://doi.org/10.1016/S0894-1777\(02\)00266-2](https://doi.org/10.1016/S0894-1777(02)00266-2)
- Chatton, E., Labasque, T., Bernardie, J., de, L., Guihéneuf, N., Bour, O., & Aquilina, L. (2017). Field continuous measurement of dissolved gases with a CF-MIMS: Applications to the physics and biogeochemistry of groundwater flow. *Environmental Science & Technology*, *51*, 846–854. <https://doi.org/10.1021/acs.est.6b03706>
- Chen, C. T., & Millero, F. J. (1977). The use and misuse of pure water PVT properties for lake waters. *Nature*, *266*(5604), 707–708. <https://doi.org/10.1038/266707a0>
- Cirpka, O., Reichert, P., Wanner, O., Müller, S. R., & Schwarzenbach, R. P. (1993). Gas exchange at river cascades: Field experiments and model calculations. *Environmental Science & Technology*, *27*(10), 2086–2097. <https://doi.org/10.1021/es00047a014>
- Deane, G. B., & Czerski, H. (2008). A mechanism stimulating sound production from air bubbles released from a nozzle. *Journal of the Acoustical Society of America*, *123*(6), EL126–EL132. <https://doi.org/10.1121/1.2908198>
- Deane, G. B., & Stokes, M. D. (2002). Scale dependence of bubble creation mechanisms in breaking waves. *Nature*, *418*(6900), 839–844. <https://doi.org/10.1038/nature00967>
- Deike, L., & Melville, W. K. (2018). Gas transfer by breaking waves. *Geophysical Research Letters*, *45*(19), 10482–10492. <https://doi.org/10.1029/2018GL078758>
- Geay, T., Belleudy, P., Gervaise, C., Habersack, H., Aigner, J., Kreisler, A., et al. (2017). Passive acoustic monitoring of bed load discharge in a large gravel bed river. *Journal of Geophysical Research: Earth Surface*, *122*, 528–545. <https://doi.org/10.1002/2016JF004112>
- Goddijn-Murphy, L., Woolf, D. K., Callaghan, A. H., Nightingale, P. D., & Shutler, J. D. (2016). A reconciliation of empirical and mechanistic models of the air-sea gas transfer velocity. *Journal of Geophysical Research: Oceans*, *121*, 818–835. <https://doi.org/10.1002/2015JC011096>
- Hall, R. O., & Madinger, H. L. (2018). Use of argon to measure gas exchange in turbulent mountain streams. *Biogeosciences*, *15*, 3085–3092. <https://doi.org/10.5194/bg-15-3085-2018>
- Hall, R. O., & Ulseth, A. J. (2019). Gas exchange in streams and rivers. *WIREs Water*, *7*(1), 1–18. <https://doi.org/10.1002/wat2.1391>
- Harjung, A., Ejarque, E., Battin, T., Butturini, A., Sabater, F., Stadler, M., et al. (2019). Experimental evidence reveals impact of drought periods on dissolved organic matter quality and ecosystem metabolism in subalpine streams. *Limnology & Oceanography*, *64*(1), 46–60. <https://doi.org/10.1002/lno.11018>
- Horgby, Å., Segatto, P. L., Bertuzzo, E., Lauerwald, R., Ulseth, A. J., Vennemann, T. W., et al. (2019). Unexpected large evasion fluxes of carbon dioxide from turbulent streams draining the world's mountains. *Nature Communications*, *10*, 4888. <https://doi.org/10.1038/s41467-019-12905-z>
- Jähne, B. J., Münnich, K. O., Bösinger, R., Dutzi, A., Huber, W., & Libner, P. (1987). On the parameters influencing air-water gas exchange. *Journal of Geophysical Research*, *92*(C2), 1937–1949. <https://doi.org/10.1029/JC092C02p01937>
- Jasper, J. J. (1972). The surface tension of pure liquid compounds. *Journal of Physical and Chemical Reference Data*, *1*(4), 841–1010. <https://doi.org/10.1063/1.3253106>
- Kantarcı, N., Borak, F., & Ulgen, K. O. (2005). Bubble column reactors. *Process Biochemistry*, *40*, 2263–2283. <https://doi.org/10.1016/j.procbio.2004.10.004>
- Klaus, M., Geibrink, E., Hotchkiss, E. R., & Karlsson, J. (2019). Listening to air-water gas exchange in running waters. *Limnology and Oceanography: Methods*, *17*(7), 395–414. <https://doi.org/10.1002/lom3.10321>
- Krall, K. E., Smith, A. W., Takagaki, N., & Jähne, B. (2019). Air-sea gas exchange at wind speeds up to 85ms<sup>-1</sup>. *Ocean Science*, *15*(6), 1783–1799. <https://doi.org/10.5194/os-15-1783-2019>
- Lakso, E. (1988). *Aeration at overflow weirs* (Vol. 1, pp. 1–104). Publications of the Water and Environment Research Institute.

- Lamont, J. C., & Scott, D. S. (1970). An eddy cell model of mass transfer into the surface of a turbulent liquid. *American Institute of Chemical Engineers Journal*, 16(4), 513–519. <https://doi.org/10.1002/aic.690160403>
- Larsen, I. J., Montgomery, D. R., & Greenberg, H. M. (2014). The contribution of mountains to global denudation. *Geology*, 42(6), 527–530. <https://doi.org/10.1130/G35136.1>
- Laursen, A., & Seitzinger, S. (2005). Limitations to measuring riverine denitrification at the whole reach scale: Effects of channel geometry, wind velocity, sampling interval, and temperature inputs of N<sub>2</sub>-enriched groundwater. *Hydrobiologia*, 545, 225–236. <https://doi.org/10.1007/s10750-005-2743-3>
- Leighton, T. G., & Walton, A. J. (1987). An experimental study of the sound emitted from gas bubbles in a liquid. *European Journal of Physics*, 8, 98–104. <https://doi.org/10.1088/0143-0807/8/2/005>
- Likens, G. E. (Ed.) (2010). *Biochemistry of Inland Waters* (1st Edition). Academic Press.
- Loewen, M. R., & Melville, W. K. (1991). A model of the sound generated by breaking waves. *Journal of the Acoustical Society of America*, 90(4), 2075–2080. <https://doi.org/10.1121/1.401634>
- McCutchan, J., Lewis, W. M., & Saunders, J. F., III. (1998). Uncertainty in the estimation of stream metabolism from open-channel oxygen concentrations. *Journal of the North American Benthological Society*, 17(2), 155–164. <https://doi.org/10.2307/1467959>
- Memery, L., & Merlivat, L. (1985). Modelling of gas flux through bubbles at the air-water interface. *Tellus*, 37B, 272–285. <https://doi.org/10.3402/tellusb.v37i4-5.15030>
- Merlivat, L., & Memery, L. (1983). Gas-exchange across an air-water-interface - experimental results and modeling of bubble contribution to transfer. *Journal of Geophysical Research: Oceans*, 88(C1), 707–724. <https://doi.org/10.1029/JC088iC01p00707>
- Miao, T., Liu, J., Qin, S., Chu, N., Wu, D., & Wang, L. (2018). The flow and acoustic characteristics of underwater gas jets from large vertical exhaust nozzles. *Journal of Low Frequency Noise, Vibration and Active Control*, 37(1), 74–89. <https://doi.org/10.1177/1461348418761688>
- Moog, D. B., & Jirka, G. H. (1999). Air-water gas transfer in uniform channel flow. *Journal of Hydraulic Engineering*, 125, 3–10. [https://doi.org/10.1061/\(asce\)0733-9429\(1999\)125:1\(3\)](https://doi.org/10.1061/(asce)0733-9429(1999)125:1(3))
- Morse, N., Bowden, W. B., Hackman, A., Pruden, C., Steiner, E., & Berger, E. (2007). Using sound pressure to estimate reaeration in streams. *Journal of the North American Benthological Society*, 26(1), 28–37. [https://doi.org/10.1899/0887-3593\(2007\)26\[28:USPTER\]2.0.CO;2](https://doi.org/10.1899/0887-3593(2007)26[28:USPTER]2.0.CO;2)
- Nezu, I., & Nakagawa, H. (1993). *Turbulence in open-channel flows*. CRC Press. <https://doi.org/10.1201/9780203734902>
- Pandit, A. B., Varley, J., Thorpe, R. B., & Davidson, J. F. (1992). Measurement of bubble size distribution: An acoustic technique. *Chemical Engineering Science*, 47(5), 1079–1089. [https://doi.org/10.1016/0009-2509\(92\)80233-3](https://doi.org/10.1016/0009-2509(92)80233-3)
- Peter, H., Singer, G. A., Preiler, C., Chiffard, P., Steniczka, G., & Battin, T. J. (2014). Scales and drivers of the temporal pCO<sub>2</sub> dynamics in an alpine stream. *Journal of Geophysical Research: Biogeosciences*, 119, 1078–1091. <https://doi.org/10.1002/2013JG002552>
- Qu, B., Aho, K. S., Li, C., Kang, S., Sillanpää, M., Yan, F., et al. (2017). Greenhouse gases emissions in rivers of the Tibetan Plateau. *Scientific Reports*, 7(1), 1–9. <https://doi.org/10.1038/s41598-017-16552-6>
- Raymond, P., Hartmann, J., Lauerwald, R., Sobek, S., McDonald, C. P., Hoover, M., et al. (2013). Global carbon dioxide emissions from inland waters. *Nature*, 503(7476), 355–359. <https://doi.org/10.1038/nature12760>
- Raymond, P. A., Zappa, C. J., Butman, D., Bott, T. L., Potter, J., Mulholland, P., et al. (2012). Scaling the gas transfer velocity and hydraulic geometry in streams and small rivers. *Limnology and Oceanography: Fluids and Environments*, 2(1), 41–53. <https://doi.org/10.1215/21573689-1597669>
- Sueur, J., Aubin, T., & Simonis, C. (2008). Seewave: A free modular tool for sound analysis and synthesis. *Bioacoustics*, 18, 213–226. <https://doi.org/10.1080/09524622.2008.9753600>
- Tokoro, T., Kayanne, H., Watanabe, A., Nadaoka, K., Tamura, H., Nozaki, K., et al. (2008). High gas-transfer velocity in coastal regions with high energy-dissipation rates. *Journal of Geophysical Research: Oceans*, 113(11), 1–14. <https://doi.org/10.1029/2007JC004528>
- Ulseth, A. J., Hall, R. O. Jr., Canadell, M. B., Madinger, H. L., Niayifar, A., & Battin, T. J. (2019). Distinct air–water gas exchange regimes in low- and high-energy streams. *Nature Geoscience*, 12, 259–263. <https://doi.org/10.1038/s41561-019-0324-8>
- Vachon, D., Prairie, Y. T., & Cole, J. J. (2010). The relationship between near-surface turbulence and gas transfer velocity in freshwater systems and its implications for floating chamber measurements of gas exchange. *Limnology & Oceanography*, 55(4), 1723–1732. <https://doi.org/10.4319/lo.2010.55.4.1723>
- Vautier, C., Abhervé, R., Labasque, T., Laverman, A. M., Guillou, A., Chatton, E., et al. (2020). Mapping gas exchanges in headwater streams with membrane inlet mass spectrometry. *Journal of Hydrology*, 581, 124398. <https://doi.org/10.1016/j.jhydrol.2019.124398>
- Vingiani, F., Durigetto, N., Klaus, M., Schelker, J., Labasque, T., & Botter, G. (2021). Evaluating stream CO<sub>2</sub> outgassing via drifting and anchored flux chambers in a controlled flume experiment. *Biogeosciences*, 18, 1223–1240. <https://doi.org/10.5194/bg-18-1223-2021>
- Wallin, M. B., Öquist, M. G., Buffam, I., Billett, M. F., Nisell, J., & Bishop, K. H. (2011). Spatiotemporal variability of the gas transfer coefficient (K<sub>CO2</sub>) in boreal streams: Implications for large scale estimates of CO<sub>2</sub> evasion. *Global Biogeochemical Cycles*, 25(3), 1–14. <https://doi.org/10.1029/2010GB003975>
- Wang, B., Liao, Q., Fillingham, J. H., & Bootsma, H. A. (2015). On the coefficients of small eddy and surface divergence models for the air–water gas transfer velocity. *Journal of Geophysical Research: Oceans*, (1), 2813–2825. <https://doi.org/10.1002/2014JC010253>
- Wang, J., Bombardelli, F. A., & Dong, X. (2021). Physically based scaling models to predict gas transfer velocity in streams and rivers. *Water Research*, 57(3), e2020WR028757. <https://doi.org/10.1029/2020WR028757>
- Wanninkhof, R. (2014). Relationship between wind speed and gas exchange over the ocean revisited. *Limnology and Oceanography: Methods*, 12(JUN), 351–362. <https://doi.org/10.4319/lo.2014.12.351>
- Wanninkhof, R., Mulholland, P. J., & Elwood, J. W. (1990). Gas exchange rates for a first-order stream determined with deliberate and natural tracers. *Water Resources Research*, 26(7), 1621–1630. <https://doi.org/10.1029/WR026i007p01621>
- Weber, U. W., Cook, P. G., Brennwald, M. S., Kipfer, R., Stieglitz, T. C., Universite, A., et al. (2019). A novel approach to quantify air–water gas exchange in shallow surface waters using high-resolution time series of dissolved atmospheric gases. *Environmental Science & Technology*, 53, 1463–1470. <https://doi.org/10.1021/acs.est.8b05318>
- Woolf, D. K. (1993). Bubbles and the air–sea transfer velocity of gases bubbles and the air–sea transfer velocity of gases. *Atmosphere-Ocean*, 31(4), 517–540. <https://doi.org/10.1080/07055900.1993.9649484>
- Woolf, D. K. (1997). Bubbles and their role in gas exchange. In P. S. Liss, & R. A. Duce (Eds.), *The sea surface and global change* (pp. 173–206). Cambridge University Press. <https://doi.org/10.1017/cbo9780511525025.007>
- Woolf, D. K., Leifer, I. S., Nightingale, P. D., Rhee, T. S., Bowyer, P., & Caulliez, G. (2007). Modelling of bubble-mediated gas transfer: Fundamental principles and a laboratory test. *Journal of Marine Systems*, 66, 71–91. <https://doi.org/10.1016/j.jmarsys.2006.02.011>
- Yoon, S. W., Crum, L. A., Prosperetti, A., & Lu, N. Q. (1991). An investigation of the collective oscillations of a bubble cloud. *Journal of the Acoustical Society of America*, 89(2), 700–706. <https://doi.org/10.1121/1.1894629>
- Zappa, C. J., McGillis, W. R., Raymond, P. A., Edson, J. B., Hints, E. J., Zemmeling, H. J., et al. (2007). Environmental turbulent mixing controls on air–water gas exchange in marine and aquatic systems. *Geophysical Research Letters*, 34(10), 1–6. <https://doi.org/10.1029/2006GL028790>

- Zeileis, A., & Hothorn, T. (2002). Diagnostic checking in regression relationships. *R News*, 2(3), 7–10.
- Zhang, W., Asce, A. M., Zhu, D. Z., & Asce, M. (2014). Trajectories of air-water bubbly jets in crossflows. *Journal of Hydraulic Engineering*, 140(7), 1–9. [https://doi.org/10.1061/\(ASCE\)HY.1943-7900.0000886](https://doi.org/10.1061/(ASCE)HY.1943-7900.0000886)
- Zhang, W., & Zhu, D. Z. (2013). Bubble characteristics of air-water bubbly jets in crossflow. *International Journal of Multiphase Flow*, 55, 156–171. <https://doi.org/10.1016/j.ijmultiphaseflow.2013.05.003>

## References From The Supporting Information

- Besagni, G., Inzoli, F., & Ziegenhein, T. (2018). Two-phase bubble columns: A comprehensive review. *Chemical Engineering*, 2(13), 1–80. <https://doi.org/10.3390/chemengineering2020013>
- Bray, D. I., & Davar, K. S. (1987). Resistance to flow in gravel-bed rivers. *Canadian Journal of Civil Engineering*, 14, 77–86. <https://doi.org/10.1139/l87-010>
- Crowther, P. A. (1988). Bubble noise creation mechanisms. In B. R. Kerman (Ed.), *Sea surface sound* (pp. 131–150). Kluwer Academic. [https://doi.org/10.1007/978-94-009-3017-9\\_11](https://doi.org/10.1007/978-94-009-3017-9_11)
- Labasque, T., Aquilina, L., Vergnaud, V., Hochreutener, R., Barbecot, F., & Casile, G. (2014). Inter-comparison exercises on dissolved gases for groundwater dating – (1) Goals of the exercise and site choice, validation of the sampling strategy. *Applied Geochemistry*, 40, 119–125. <https://doi.org/10.1016/j.apgeochem.2013.11.007>
- Lu, N. Q., Prosperetti, A., & Yoon, S. W. (1990). Underwater noise emissions from bubble clouds. *IEEE Journal of Oceanic Engineering*, 15(4), 275–281. <https://doi.org/10.1109/48.103521>
- Medwin, H. (1975). Speed of sound in water: A simple equation for realistic parameters. *Journal of the Acoustical Society of America*, 58(6), 1318–1319. <https://doi.org/10.1121/1.380790>
- Minnaert, M. (1933). On musical air-bubbles and the sounds of running water. *The London, Edinburgh and Dublin Philosophical Magazine and Journal of Science*, 16(104), 235–248. <https://doi.org/10.1080/14786443309462277>
- Nikora, V. I., & Smart, G. M. (1997). Turbulence characteristics of New Zealand gravel-bed rivers. *Journal of Hydraulic Engineering*, 123(9), 764–773. [https://doi.org/10.1061/\(asce\)0733-9429\(1997\)123:9\(764\)](https://doi.org/10.1061/(asce)0733-9429(1997)123:9(764))
- Sugisaki, R., & Taki, K. (1987). Simplified analyses in of He, Ne, and Ar dissolved in natural waters. *Geochemical Journal*, 21, 23–27. <https://doi.org/10.2343/geochemj.21.23>